Microporous and Mesoporous Materials 211 (2015) 64–72

Contents lists available at ScienceDirect

Microporous and Mesoporous Materials

journal homepage: www.elsevier.com/locate/micromeso

Secondary growth of ZIF-8 films onto copper-based foils. Insight into surface interactions

Rocío L. Papporello, Eduardo E. Miró, Juan M. Zamaro*

Instituto de Investigaciones en Catálisis y Petroquímica, INCAPE (FIQ, UNL, CONICET), Santiago del Estero 2829 (3000), Santa Fe, Argentina

ARTICLE INFO

Article history:
Received 10 October 2014
Received in revised form
23 February 2015
Accepted 25 February 2015
Available online 5 March 2015

Keywords:
ZIF-8 coating
Secondary synthesis
Solvothermal growth
Copper
Surface chemistry

ABSTRACT

The film growth of the zeolitic imidazolate framework-8 on a copper-based substrate is reported for the first time in the literature. The growth mechanism on copper foils is analyzed, and it is demonstrated that during synthesis the development of the metal-organic framework (MOF) film is sensitive to the interactions produced between the support surface, the solvent and the reactants. In order to compare the surface interactions during synthesis, Fecralloy foils, porous alumina disks and macroporous cordierite monoliths are also analyzed. The physicochemical properties of the materials are evaluated by XRD, SEM, EPMA, AAS, DRIFT and XPS. In dimethylformamide-based media, no ZIF-8 film develops on the copper surface due to unfavorable interactions that make its growth non selective. At the same time, the formation of a dense ZnO layer is favored, this layer being promoted by decomposition products of the solvent and the zinc reagent. When water-based media are used, those interactions are modified thus avoiding the formation of oxide, but the growth kinetics of the ZIF-8 film is still low. On the other hand, when using mixtures based on methanol with the addition of acetate, continuous, uniform, and adherent ZIF-8 films can be obtained. Such films develop preferential crystallographic orientations in planes {200} and {110}, have thicknesses between 5 and 10 microns and good mechanical and thermal stability. The results obtained provide a platform for the obtention of ZIF-8 films on copper structures, which is relevant for the development of new structured catalysts based on MOFs.

1. Introduction

The study and application of metal-organic frameworks (MOFs) has widely increased in recent years because these materials present great design flexibility in terms of their porous architecture, which ranges from the microporous to the mesoporous scale [1]. MOFs are crystalline solids which consist of inorganic clusters linked by organic ligands in three-dimensional arrangements and offer a unique chemical versatility, high internal porosity and properties that are different from those of traditional porous materials such as zeolites, porous silicas, or activated carbon. Having hydrophilic and hydrophobic areas coexisting within the pores and influencing their adsorption properties, and flexible structures that show breathing and gate effects where the pores open or contract during the diffusion of molecules are only two of these advantageous properties [2]. For these reasons, MOFs have a wide range of potential applications in different fields such as adsorption [3], gas separation by membranes [4,5], controlled drug release [6], sensors [7] and catalysis [8]. In the latter field, most studies have focused on liquid phase catalysis and, to a lesser extent, on gas–solid heterogeneous reactions [9].

A MOF family of potential interest is that of zeolitic imidazolate frameworks (ZIFs) since they present good thermal and chemical stability [10]. Particularly, ZIF-8 presents a high specific surface area (1000–1600 $m^2\ g^{-1}$), thermal stability up to temperatures close to 400 °C and good chemical stability in water, alkaline solutions and organic solvents [11].

The architecture of ZIF-8 is based on Zn^{2+} atoms linked to nitrogens of imidazolate anions at connection angles close to 145° in tetrahedral coordination, forming a three-dimensional network with a zeolitic topology (SOD type) with cavities of 11.6 Å, accessible through windows of 3.4 Å [11]. However, their structure is flexible and allows the entry of molecules that are bigger than this window size [12].

Supported microporous ZIF-8 films have been studied mainly for gas separation applications, so that the supports used have been

* Corresponding author. Tel./fax: +55 0342 4536861.
E-mail address: zamaro@fiq.unl.edu.ar (J.M. Zamaro).

http://dx.doi.org/10.1016/j.micromeso.2015.02.049
1387-1811/

porous ceramic materials such as porous alumina in the shape of discs or tubes [13–29]. Other supports on which ZIF-8 films have been synthesized include glass slide [30], polysulfone membrane [31], carbon nanotube bucky-paper [32], nylon membrane [33], silicon [34] and polymide [35]. Our interest is to synthesize MOF films on appropriate substrates so as to allow their utilization as structured catalysts in processes with a high demand of heat transfer. To the best of our knowledge, no studies on the synthesis of ZIF-8 films on metallic supports with high thermal conductivity and diffusivity such as copper or copper alloys [36,37] have been reported so far. This type of supports has successfully been applied in zeolite film-based microreactors for the oxidation of CO [38]. The aim of this work is, therefore, to study the interactions occurred during the secondary synthesis of ZIF-8 films on the surface of copper-based foils with a view to supplying useful information for the development of novel structured catalysts based on these microporous-phase films.

2. Experimental

2.1. Support pretreatments

Foils of electrolytic copper (99.9% purity) 50 microns thick and brass foils (Cu:Zn = 65:35) 100 microns thick were used. In order to analyze the surface interactions during synthesis, Fecralloy® foils 50 micron thick (Goodfellow), porous α-alumina disks (Inocermic, thickness 2 mm, average pore diameter 1.8 μm) and macroporous cordierite monoliths (Corning, 400 cps) were employed as substrates. Metallic foils were cut into 2 × 1 cm pieces, washed thoroughly with soapy water and rinsed. Then, the surface was sanded for 1 min with fine abrasive paper on both sides. The Fecralloy substrate was the only support which was previously calcined in a muffle at 900 °C for 22 h in order to generate a surface layer of alumina [39]. The other supports were not calcined previously to the ZIF-8 synthesis. The ceramic substrates were not sanded since their porous nature allows a good retention of seed crystals. Subsequently, all supports were subjected to an ultrasonic bath, first in water and then in acetone and finally dried and seeded. The latter was done manually by rubbing ZIF-8 nanocrystals (Basolite Z1200®, Sigma–Aldrich) using latex gloves, making circular movements for 1 min on both sides of the foils while the excess of crystals was removed by the gentle brushing of the surface.

2.2. Synthesis methodology

For the secondary synthesis treatments, protocols based on dimethylformamide [11], methanol [17] and water [40] were used The reaction mixture consisted of dimethylformamide (DMF, Sigma–Aldrich, 99.0%), 2-methylimidazole (mim, Sigma–Aldrich) and $(NO_3)_2Zn\cdot 6H_2O$ (Sigma–Aldrich) in a molar ratio of Zn:mim:DMF = 1:1:129. For the water-based protocol, the same reagents were used in a molar ratio of Zn:mim:H_2O = 1:57:4552. In the case of mixtures of methanol (Cicarreli pro-analysis), sodium acetate (Ac) was added (Cicarreli pro-analysis) with molar ratios of Zn:Ac:mim: methanol = 1:x:2:200 (where x = 0, 1, 2, 4 and 8). The solutions of mim and Zn^{2+} were prepared separately in the respective solvent under stirring and, subsequently, both solutions were mixed and placed in a teflon vessel together with the substrate in vertical position to minimize the settling of crystals nucleated in solution during synthesis. Then, synthesis treatments were carried out in an autoclave varying the temperatures and times (30 °C–140 °C, 2 h–48 h). Later, the substrates were removed, rinsed with water to remove residual reagents and/or loosely adhered deposits and finally dried at 120 °C for 24 h.

2.3. Characterizations

In order to study the crystalline structure of the films and their thermal stability, X-ray Diffraction (XRD) was performed, both at room temperature and with programmed temperature (TXRD). Room-temperature studies were conducted with a Shimadzu XD-D1 instrument by scanning the 2θ angle at 2° min^{-1} between 5° and 50° (CuKα radiation, λ = 1.5418 Å, 30 kV, 40 mA), while studies in temperature were performed, using the same scanning conditions, in a Bruker D8 Advance diffractometer equipped with a Lynx eye detector in flowing He between 200 °C and 500 °C and taking measurements after 15 min of stabilization at each temperature. Diffuse Reflectance Infrared Spectroscopy (DRIFT) in temperature was performed with a Bruker Equinox 55 with MCT detector. The sample was placed in the chamber with He flow and the measurement started with a ramp of 5 °C min^{-1} to 400 °C, acquiring spectra at 5–10 min intervals and taking the spectrum of a polished aluminum sample as background. The quality and microstructure of the films were examined by Scanning Electron Microscopy (SEM) with a JEOL JSM-35C operated at 20 kV. The samples were glued to the sample holder with Ag painting and then coated with a thin layer of Au in order to improve the images. In order to study the distribution of the chemical elements present in the films, Electron Probe Microanalyses (EPMA) were performed with a dispersive EDAX equipment coupled to the SEM instrument. The Atomic Absorption Spectroscopy (AAS) of the liquids was performed with a Perkin Elmer 800 Analyst with flame atomization. The surface composition was examined by X-ray Photoelectron Spectroscopy (XPS) with a Multitechnique Specs module. The binding energies (BE) of Zn 2p, C 1s, N 1s, O 1s and Cu 2p core-levels were analyzed. The kinetic energy (KE) in the LMM region of the Zn Auger transitions was also analyzed. The spectra were obtained with a pass energy of 30 eV with a Mg anode operated at 200 W. The foils were supported on the sample holder, subjected to vacuum dehydration at 150 °C for 15 min and finally evacuated under vacuum prior to the readings. The peak of C 1s at 284.8 eV was taken as internal reference. Data processing was performed using the Casa XPS software.

3. Results and discussion

3.1. Synthesis employing dimethylformamide (DMF) as solvent

3.1.1. Synthesis on metallic supports

The procedure employed for the synthesis of ZIF-8 crystals presents an evident analogy with those used to obtain other microporous materials like zeolites. With respect to the growth of zeolite films over different types of supports, it is generally accepted that the same synthesis solutions used to develop crystals can be used to grow zeolite films. However, this is not the case of ZIF-8. As a matter of fact, until now the original procedure with dimethylformamide (DMF) used as solvent for the synthesis of crystals [11] has not been reported for film growth. Only one work has been published so far, but this study uses a modified procedure that employs DMF with triethylamine [29]. In what follows, we describe our experiments and findings about the application of the protocol used for powder synthesis to the growth of ZIF-8 films on copper-based foils.

Figs. 1 and 2 show XRD patterns and SEM images, respectively, that correspond to syntheses performed on different supports. These results will be analyzed for each case. Fig. 1b depicts the XRD pattern obtained for the synthesis carried out on the brass support employing the protocol that uses DMF. Peaks at 2θ: 47.6°, 36.4°, 34.5° and 31.9° (asterisks) correspond to a ZnO phase (JCPDS 5-664), while those at 2θ: 49.74° and 42.63° (circles) are due to the

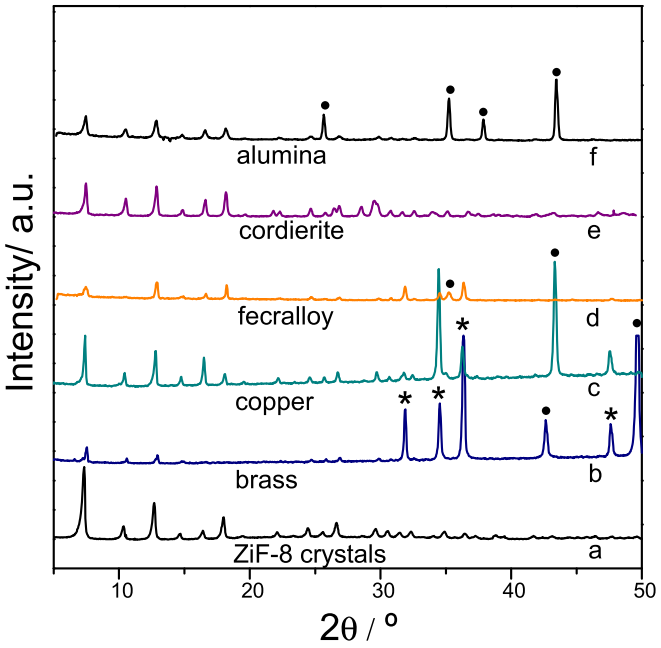

Fig. 1. XRD patterns of supports after solvothermal treatments in DMF-based syntheses: a) ZIF-8 seeding crystals, b) brass foil; c) copper foil, d) pretreated Fecralloy foil, e) cordierite monolith, f) porous alumina disc.

support (JCPDS 3-1015). Meanwhile, the signals observed at lower angles (2θ: 7.4°, 10.4° and 12.7°) are the main features associated with the ZIF-8 phase [11], which are the same as those obtained for the seed nanocrystals (Fig. 1a). The low intensity of the ZIF-8 signals developed on the brass foil indicates that a scarce amount of crystals is present on this support. On the contrary, the powder recuperated from the synthesis solution presents ZIF-8 as the main product (Fig. S1a). After the synthesis, the surface of the brass foil (Fig. 2a) presents an aspect totally different from that of the seeded support (Fig. S2a), showing a dense and continuous film that totally covers the substrate. The said coating, constituted by an intergrown, dense film of polyhedral crystals, is 3 μm thick (Fig. 2b). On the other hand, on the top of some zones of this film, big dodecahedral crystals of ZIF-8 were observed. Most probably, these crystals were formed in the solution synthesis and then deposited on the top of the grown film. EPMA analyses performed on a cross section of the film (as depicted in Fig. 2b) show Cu and Zn in the regions close to the support (Table 1). Meanwhile, near the surface, the proportion of oxygen increased and that of copper decreased. The atomic proportions confirm that the continuous film is constituted by ZnO. Since brass contains Zn in its composition, the ZnO film could be formed, at least in part, taking Zn from the metallic foil. To gain further insight into this possibility, the synthesis process on pure copper substrates was analyzed.

Copper foils were subjected to the same synthesis protocol described above, using DMF as solvent. Again, XRD signals corresponding to ZIF-8 and ZnO phases were observed (Fig. 1c). Although a development of a ZIF-8 film was not produced, big isolated crystals adhered to a dense ZnO film were detected (Fig. 2c), similarly to what was observed on brass foils. The different chemical compositions between the continuous film and the deposited crystals are evidenced by the contrast in the backscattered image (Fig. S2b). The surface of the film (Table 1) contains Zn and O with an atomic ratio that corresponds to a ZnO phase, in agreement with XRD results. The Cu and Zn distribution is shown in the mapping of the film cross-section (Fig. 2d) and a migration of copper from the support towards the ZnO film is noteworthy.

The presence of the ZnO film onto the copper surface clearly indicates that the source of Zn comes from the synthesis solution and its growth prevails against the growth of the ZIF-8 film. Since this behavior could be related to interactions between reactants and the metallic surface, synthesis onto non-metallic surfaces were carried out. Fecralloy® foils were chosen because alumina whiskers develop after a thermal treatment at high temperature, thus generating a non-metallic interphase. Ceramic substrates were also used, as discussed in the following section.

3.1.2. *Syntheses on supports with non-metallic surfaces*

When a thermally treated Fecralloy support was used, weak XRD signals of ZIF-8 were developed (Fig. 1d) from isolated crystals formed in the solution and deposited on the foil (Fig. S2c), together with some overlapped peaks from ZnO. The EPMA analyses on the support surface showed small amounts of Al and Zn associated with the said oxides as well as signals of Fe and Cr coming from the support (Fig. S3b). An important result is that in this case, a ZnO phase was only scarcely developed, probably as dispersed and isolated deposits. Most probably, the alumina surface does not constitute a compact barrier between the solution and the alloy, some contact of reactants with the metal surface takes place, and some small extent of ZnO formation occurs.

When the synthesis in DMF was performed onto totally ceramic substrates as cordierite and α-alumina, only a ZIF-8 pure phase developed, and ZnO was not observed (Fig. 1). While the cordierite monolith surface shows a conglomerate of ZIF-8 crystals induced by the seeded ones (Fig. S2d), a high amount of crystals grows inside the channels due to the direct synthesis processes (Fig. S2d). On α-alumina the MOF growth was developed as a continuous film constituted by packed crystals (Fig. S2e) of 2 μm thickness (Fig. S2f). In both supports ZnO was neither produced on the surface nor in the powder recovered from the synthesis solution. These results confirm that the contact between the solution and the metallic surfaces play a fundamental role in the ZnO layer formation.

The solvent could modify both the evolution of the ZIF-8 crystals formation [41] and the chemistry at the substrate surface. In order to better understand the effects of the solvent, the synthesis process on pure copper supports was carried out using water and methanol, respectively, and the results are described below.

3.2. *Synthesis employing water or methanol as solvents*

Copper foils were subjected to a synthesis in a water-based mixture at 30 °C during 6 h. After that, weak ZIF-8 XRD peaks developed, but ZnO signals were absent (Fig. S1f). Small crystals immersed into a thin layer that partially covers the copper surface were observed (Fig. 2e) and the marks generated during the sanding process could be still appreciated. The different results obtained compared to those observed when using DMF evidences the important role exerted by the solvent in the zinc oxide formation. Besides, some degree of copper dissolution takes place, as evidenced by the blue color of the solution after the synthesis. The amounts of copper in solution were determined and they are shown in Table 2. It can be observed that the copper concentration increased when the synthesis time increased from 6 h to 24 h, but for higher times it remained constant. The intensity of the XRD peaks was similar for synthesis times of 24 h and 48 h, and the surfaces (Fig. 2f) presented a similar appearance to that of the sample with the lower synthesis time. The only difference was the evolution of a foamier surface originated by the dissolution of copper, as seen by AAS (Table 2). In order to favor the kinetics of the growth of ZIF-8 crystals onto the substrates surface against the copper dissolution process, syntheses at 120 °C were performed but, unfortunately, both surface structure and support leaching

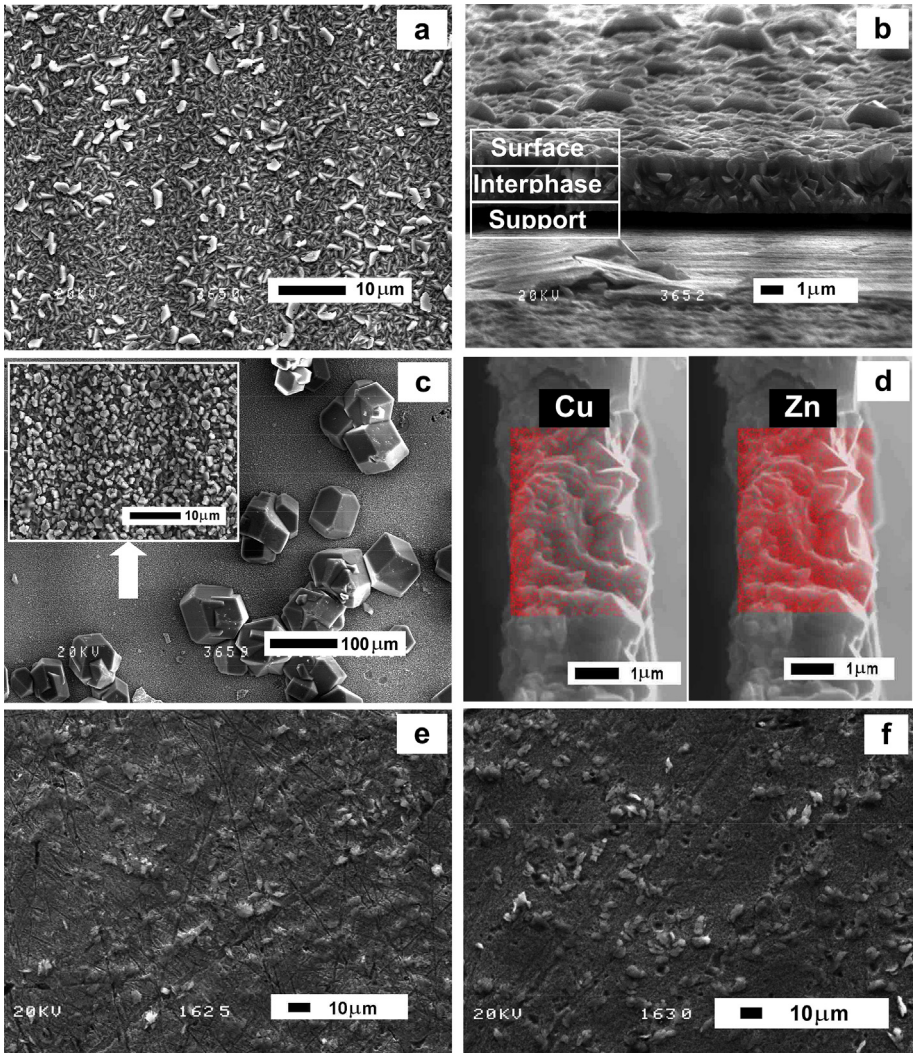

Fig. 2. SEM images of the surface of copper-based foils subjected to solvothermal treatments. Synthesis in DMF: a) brass foil in top view, b) brass foil in cross section, c) copper foil in top view, d) mapping in the cross section of the film on copper foil for details see the online version. Synthesis in water: e) copper surface after 6 h; f) copper surface after 24 h.

degree were similar to those obtained at the lower temperature (Table 2).

In order to better understand the effect of the solvent, we decided to use methanol instead of water; sodium acetate was also introduced in order to improve the ZIF-8 growth process. The addition of sodium acetate was decided taking into account the findings published elsewhere [15,42]. In this vein, the reacting mixture used had a Zn:Ac:mim ratio of 1:2:2, and after a 6 h treatment the support clearly showed ZIF-8 XRD peaks (Fig. 3b) which gained in intensity when the synthesis time increased to

Table 1
Elemental composition (by EPMA analyses) in the cross section of the films developed on copper and brass supports using DMF as solvent.

Element[a]	Brass			Copper
	Surface	Interphase	Support	Surface
Cu	3.73	32.52	58.44	3.09
Zn	52.88	49.71	27.30	52.31
O	43.39	17.76	14.27	44.6

[a] Atomic percent.

Table 2
Copper leached from supports (by AAS analyses) after the solvothermal treatments in water-based and methanol-based syntheses.

Water-based syntheses		
Time (h)	Temperature (°C)	Cu in sol. (ppm)
6	70	24
24	70	67
48	70	65
6	120	66
24	120	71
48	120	71
Methanol-based syntheses		
Time (h)[a]	Zn:Ac:mim[b]	Cu in sol. (ppm)
12	1:2:2	147
16	1:2:2	134
24	1:2:2	286
12	1:1:2	280
12	1:4:2	46
12	1:8:2	41

[a] The syntheses were performed at 120 °C.
[b] Molar proportions of reactives.

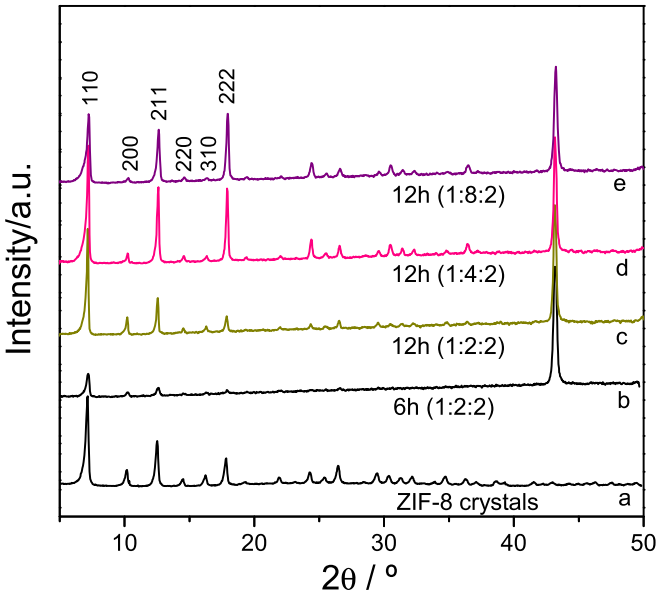

Fig. 3. XRD patterns of the copper foils treated with the methanol-based protocol: a) ZIF-8 seeding crystals, b) 6 h with Zn:Ac:mim 1:2:2, c) 12 h with Zn:Ac:mim 1:2:2, d) 12 h with Zn:Ac:mim 1:4:2, e) 12 h with Zn:Ac:mim 1:8:2.

12 h (Fig. 3c). An inspection of the surface after 6 h of synthesis time reveals a total coverage of the support by a continuous MOF film (Fig. 4a) which had a thickness of about 5 μm (Fig. 4b). As observed in Fig. 4c, the average size of the crystals at the surface increased with the synthesis time from about 4 μm (6 h) to 9 μm (12 h), and the film thickness also evolved reaching about 10 μm (Fig. 4d). During these syntheses, a partial dissolution of the support took place (Table 2), similar to the one observed when water was used as solvent. The dissolution also increased with the synthesis time but, as observed in the pictures shown above, the growth of the ZIF-8 film was favored. When a lower concentration of sodium acetate was used (Zn:Ac:mim = 1:1:2), there was no growth of the ZIF-8 film and, at the same time, the dissolution of copper increased (Table 2). It has been proposed that the addition of a formiate salt improves the growth of ZIF-8 crystals due to the combined effects of competition with the ligand and increase of the kinetics of growth. This latter factor is originated by a higher deprotonation of the terminal ligands at the growing crystal surface. Consequently, it stands to reason that the addition of higher proportions of acetate should result in the growth of bigger crystals at the copper surface. In order to corroborate this, experiments with higher acetate proportions were performed. When 1:4:2 or 1:8:2 Zn:Ac:mim ratios were used, the corresponding XRD patterns of the foils exhibited intense signals of ZIF-8 (Fig. 3d and e). These phases were developed as continuous films at the substrate surface which presented a higher intergrowth and average crystal size as compared with the synthesis carried out with a 1:2:2 ratio (Fig. 4e). Moreover, the increase in acetate concentration from 1:2:2 to 1:4:2 resulted in a decrease of the copper dissolved (Table 2) and in an increase of the film thickness, which reached c.a. 17 μm (Fig. 4f). The subsequent increase in acetate concentration (1:8:2) changed neither the copper dissolution nor the microstructural properties or film thickness. A close observation of the XRD patterns of these samples (Fig. 3d and e) reveals the development of a preferred crystallographic orientation of the ZIF-8 films. As a matter of fact, the relative intensities of several peaks in the diffractograms are different if compared with those of the powder crystals, which present random orientations. This effect is frequently observed in zeolite films obtained by secondary growth and could also influence their performance in processes that are sensitive to the porous topology, as adsorption or catalytic reactions [43]. The said preferential orientations can be characterized by means of a crystallographic preferential orientation index (CPO), which compares the ratio of the integrated intensities of a pair of XRD peaks of the film with the intensities of the same planes in the powder material (please see equation of CPO at the bottom of Table S1) [44]. The CPO (110/200) and CPO (211/200) were defined and, in both cases, when they approximated zero, the crystallographic orientation of the {110} and {211} planes tended to those existing in the powder. On the contrary, when these CPO tend to unity, those planes are oriented parallel to the substrate surface. The increase in the relative intensities of the {110} and {211} planes are reflected in the CPO values. For the sample prepared with Zn:Ac:mim equal to 1:4:2, the CPO (110/200) was 0.62 and the CPO (211/200) was 0.44. Meanwhile, for the 1:8:2 sample, the indexes were 0.68 and 0.47, respectively. In this vein, Bux et al. [26] observed a strong crystallographic orientation in ZIF-8 films developed on porous alumina, but in that case the orientation was for the {200} planes. The crystallographic orientations of the ZIF-8 films on copper foils are in agreement with the crystal arrangements observed. ZIF-8 crystals have dodecahedral shapes in which some faces correspond to the {110} planes and some edges correspond to the {211} planes [26]. In the front view of the films (Fig. 4e), a high proportion of the said edges and planes disposed parallel to the support can be observed.

3.3. Interactions between support surface, solvent and reactives

It is recognized that the secondary synthesis method, in principle, has the advantage relative to the direct in-situ synthesis that allows decoupling the nucleation process in the support, promoting the development of continuous films as has been widely reported for zeolite films [45]. However, the results discussed above indicate that for the growth of the ZIF-8 film by secondary synthesis to be successful, there are also other key factors playing a role such as the physicochemical interactions during synthesis in which the chemical nature of the support, the solvent and the reagents are involved. When using DMF as solvent, ZnO films on the surfaces of copper and brass were formed and this oxide acquired a positive zeta potential in alkaline solutions [46]. Furthermore, the state of electrical charges on the ZIF-8 growing surfaces can be estimated as that of suspensions of crystals of this MOF [42]. Then, our speculation is that the non-selectivity for the growth of the ZIF-8 film should be related to unfavorable electrostatic effects. Considering this argument, the result on the Fecralloy substrate with the alumina interface (where only a scarce amount of ZnO grew) suggests an effect by the contact between the metal surface and the DMF-based mixture. However, the alumina surface of this support is not totally dense and there are also small amounts of zinc oxide that may yet generate unfavorable electrostatic environments that hinder the selective growth of a ZIF-8 film. Following this reasoning, the high selectivity for the formation of the ZIF-8 films on ceramic surfaces is consistent with the fact that the surface of both cordierite [47] and porous α-alumina [48] has negative charges in alkaline solutions.

DMF syntheses on copper-containing substrates show an effect between the surface and the synthesis mixture to produce a surface ZnO film from the reactive zinc source. DMF decomposes at high temperatures with the formation of carbon monoxide and dimethylamine [49] and the latter has a strong characteristic fishy smell, which was confirmed when the autoclaves were opened at every synthesis performed with this solvent. Additionally, when these syntheses were performed in DMF without the addition of methylimidazole, ZnO was produced whereas this did not occur when water mixtures were used (Fig. S1d and e). We propose a plausible

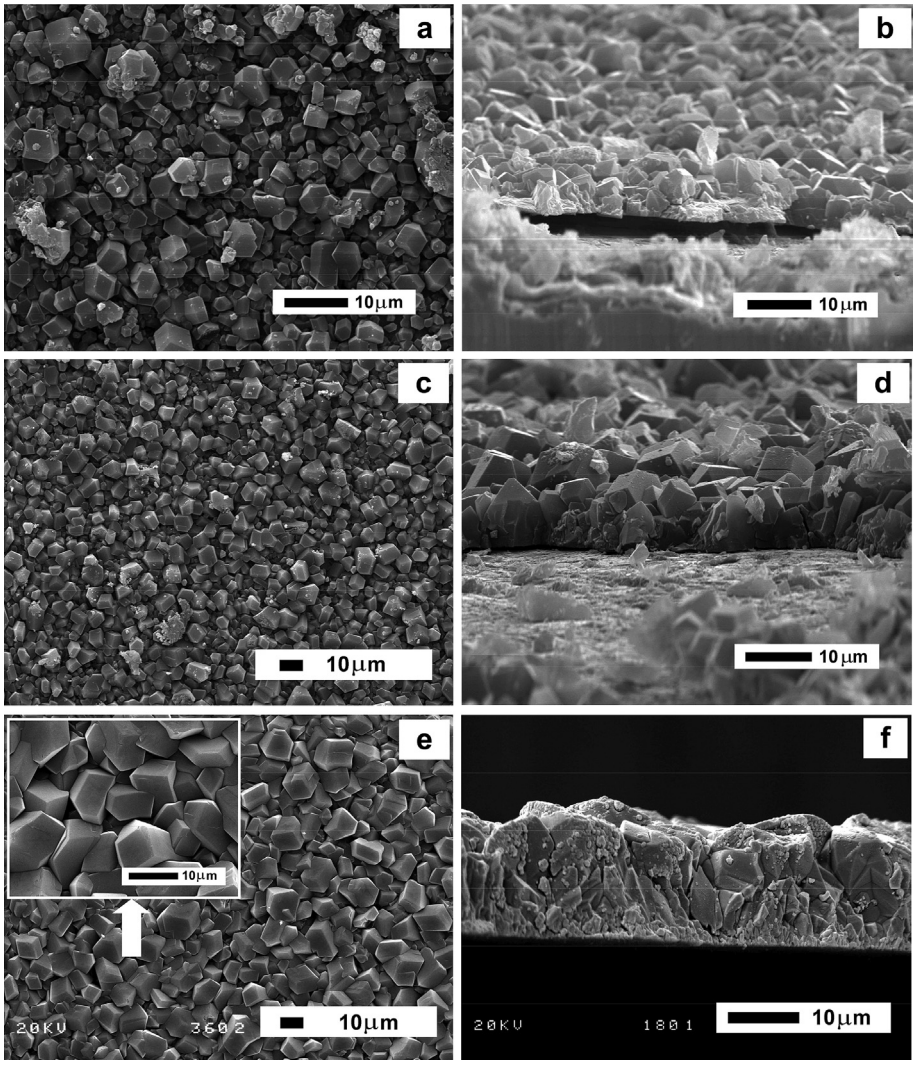

Fig. 4. SEM images of copper foils treated with the methanol-based protocol: a) 6 h with Zn:Ac:mim 1:2:2 in top view; b) 6 h with Zn:Ac:mim 1:2:2 in side view: c) 12 h with Zn:Ac:mim 1:2:2 in top view; d) 12 h with Zn:Ac:mim 1:2:2 in side view, e) 12 h with Zn:Ac:mim 1:4:2 in top view, f) 12 h with Zn:Ac:mim 1:4:2 in side view.

mechanism for the formation of the ZnO layer as shown in the scheme of Fig. 5a. The amine from DMF decomposition would facilitate the formation of zinc complexes from the zinc reagent in solution, which can be adsorbed on the surface of the copper-based substrates, similarly to what happens when such metals are subjected to NH_3 vapors [50]. Subsequently, the amino groups of the adsorbed complex may be replaced by OH^- to form $Zn(OH)_2$ which is then decomposed into ZnO during the solvothermal treatment. Additionally, some Zn^{2+} in solution also reacts with methylimidazole yielding ZIF-8 crystals in solution.

When using both water or methanol mixtures, developed ZIF-8 phases were obtained in solution and the greater selectivity of the ZIF-8 film growth in methanol should be associated with interactions in the nearby copper surface. Cravillon et al. [42] reported that an excess of neutral mim species in the synthesis mixture can act as capping agents of the growing ZIF-8 crystals because the surface terminal ligands have a low extent of deprotonation, facilitating the finalization of the crystal growth. Taking this into account, Mc Carthy et al. proposed that by adding sodium formate linkers, the surface of ZIF-8 crystals is fully deprotonated [15] which gives a larger crystal growth. In line with this claim, in our synthesis with acetate, ZIF-8 nuclei with highly deprotonated surfaces will be generated ie. with a high density of negative electrical charges. Moreover, the state of charges at the surface of the copper support can be estimated taking into account those of metallic copper, copper oxides and hydroxides, which have high pH values for the IEP (isoelectric point) of about 9.5 [51]. This situation favors the interaction between the copper surface and ZIF-8 nuclei and thus allows the development of the ZIF-8 film as shown in Fig. 5b. The results obtained when water was used as the solvent are also in agreement with the proposed mechanism. As a matter of fact, in this case the measured pH of the synthesis mixture was 9.5, and for this value the Zeta potential of ZIF-8 nuclei in aqueous suspension is of about +20 mV (Fig. S4). Thus, in this case the film growth is not favored.

3.4. Surface composition and stability of ZIF-8 films

The ZIF-8 films obtained on copper foils exhibit a surface elemental composition according to the said microporous phase. All films synthesized with different acetate ratios show XPS signals in the Zn $2p_{3/2}$ and Zn $2p_{1/2}$ regions with binding energies (BE) around 1021.4 and 1044.5 eV, respectively (Fig. 6 left), compatible with Zn^{2+} of the ZIF-8 structure as seen in crystals of this MOF [52].

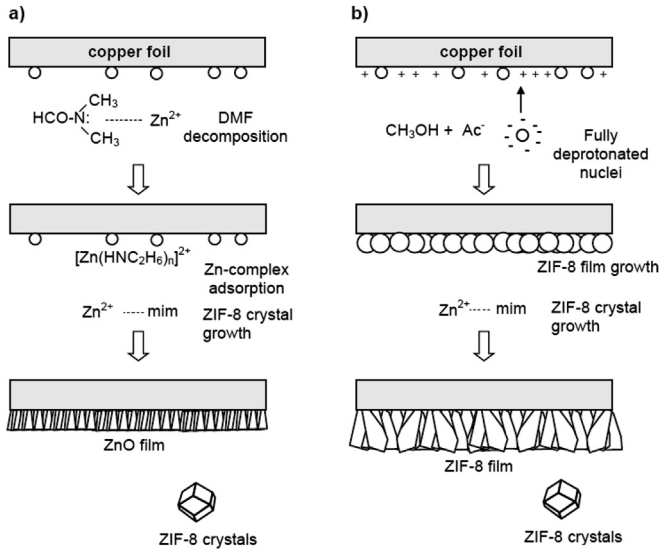

Fig. 5. a) Scheme of the proposed mechanism for ZnO film formation onto copper-containing substrates in DMF-based synthesis, b) scheme of the ZIF-8 growth on copper substrates in methanol-based synthesis.

These species were confirmed by analyzing the Auger spectra in the Zn LMM region (Fig. 6 right), which showed characteristic signals at KE around 987.5 eV [52]. This value differ from values for metallic zinc and zinc oxide which are located at higher KE [53]. When analyzing the C1s and N1s regions (Fig. S5), symmetrical signals around 398.7 eV for N1s and 284.8 eV for C1s were found which are consistent with N and C of the ligand [54]. Moreover, signals of Cu $2p_{3/2}$ centered at 932.2 eV which are typical of Cu^{1+} (Fig. S5), were found and no satellite peaks characteristic of Cu^{2+} were observed [55]. These surface copper species are in low proportion (Table 3) and probably come from the dissolution of the support during synthesis. O1s signals around 531.0 eV were also observed which are shifted with respect to that of oxygen from ZnO at 529.7 eV [55] and are associated with acetate species adsorbed at the surface of

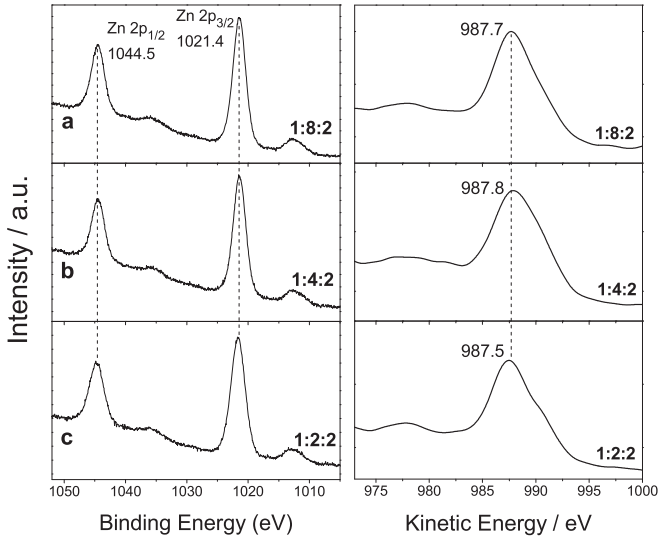

Fig. 6. XPS spectra in the Zn2p region (left) and Auger spectra in the Zn LMM region (right) of samples synthesized in methanol with different Zn:Ac:mim ratios: a) 12 h with Zn:Ac:mim 1:8:2, b) 12 h with Zn:Ac:mim 1:4:2, c) 12 h with Zn:Ac:mim 1:2:2.

Table 3
Elemental surface composition of ZIF-8 films obtained with different Zn:Ac:mim ratios as determined by XPS.

Sample	N/Zn	C/Zn	C/N	Cu/Zn
1:2:2	1.80	6.14	3.42	0.08
1:4:2	1.97	5.97	3.03	0.85
1:8:2	2.01	6.09	3.02	0.14

the ZIF-8 films. This is confirmed by calculating the C/N atomic ratio that should be 2 and in all cases was about 3 (Table 3). As mentioned above, the acetate intervenes in the formation mechanism of the film as a competitive ligand on the surface of the growing crystals. Additionally, since the theoretical N/Zn and C/Zn atomic ratios should be 4 and 8, respectively, the calculated values (Table 3) indicate a surface enrichment with zinc.

On the other hand, the ZIF-8 films had good adhesion since they were not detached by handling during the cutting performed to the SEM studies. Additionally, the films analyzed by XPS were subjected to an ultrasonic cleaning in methanol for 5 min and it was observed that the films remained firmly bonded to the substrate. However, taking into account that possible applications of the systems studied in this work belong to the field of catalysis, a more specific and rigorous stability test was designed besides the standard ultrasound test mentioned above. The synthesized sample was subjected to an ultrasound test in acetone bath during 15 min. The mass loss was measured together with the microscopic observation of the damage caused at the surface. On the other hand, thermo-mechanical stability was evaluated subjecting a sample to thermal stress by sharply cycling temperature between 250 °C and 25 °C, ten times. After that the ultrasound test was performed again and the surface was inspected. The temperature range for cycles was selected in view of a possible application, which is CO preferential oxidation (COProx). The mass loss in both cases was negligible (in the order of the error of the balance) and no damage or erosion was observed on the coating surface (Fig. S6). This implies a very good adhesion of the ZIF-8 coatings to the copper surface.

With regard to the intrinsic thermal stability of the films, although there are data for ZIF-8 crystals that were determined mainly by TGA, the behavior of this phase as a film on a substrate of high thermal conductivity may be different. Therefore, TXRD and DRIFT studies were conducted. In Fig. 7a, it can be seen that at room temperature the most representative XRD signals of the MOF at $2\theta = 7.4°$, 10.4°; 12.7° and 18.0° are present and remain unchanged when the sample is brought up to 350 °C and even after keeping it at that temperature for 1 h (350-1). However, when the temperature reached 400 °C, a slight decrease in the intensity of all XRD signals began, indicating the start of the collapse of the MOF film structure which is manifested fully at 450 °C. Fig. 7b shows the DRIFT spectra of the ZIF-8 film on copper foil on a temperature ramp. In the sample with the ZIF-8 film, the typical signals of this MOF were observed at room temperature, which mostly correspond to vibration modes of the imidazolate ring [11] as observed in the ZIF-8 powder (Fig. 7b). By increasing the temperature all signals are maintained, indicating the stability of the bonds in ZIF-8 to about 380 °C from which the bond structure begins to collapse. Finally, after spending an hour at 400 °C (400-1), a spectrum similar to the uncoated copper foil was reached. The TXRD and DRIFT results show that the maximum temperature at which these ZIF-8 films on copper foils could be used without losing their physicochemical characteristics is about 350 °C. Such limits are compatible with gas-phase reactions at moderate temperatures, like CO oxidation, in which these films, suitably functionalized, could be applied as structured catalysts. The search for new catalytic phases

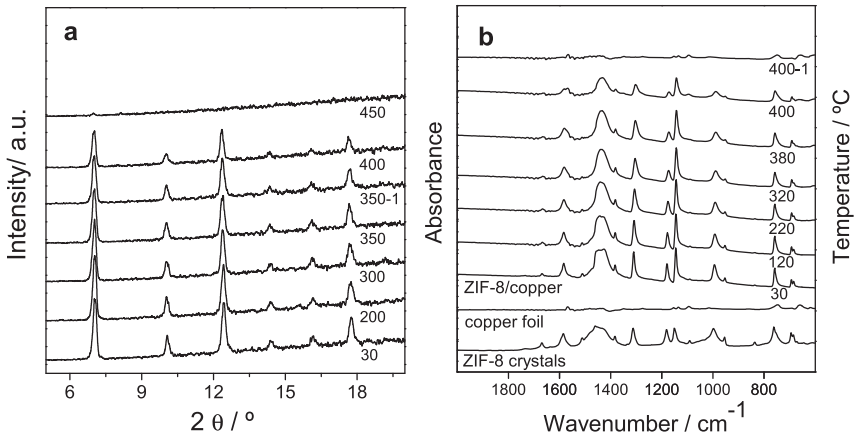

Fig. 7. Thermal evolution of the ZIF-8 film on copper foil: a) temperature-programmed XRD patterns (TXRD), b) temperature-programmed DRIFT spectra.

in the form of films is one of the tools to achieve better performances in catalytic processes and, in this sense, the use of MOF films can play an important role.

4. Conclusions

The growth of zeolitic imidazolate framework-8 (ZIF-8) films on copper-based foils was investigated. Synthesis protocols using different solvents as dimethylformamide (DMF), water and methanol on different supports were analyzed. By employing DMF no ZIF-8 film growth on copper-based supports was achieved, while the formation of a dense layer of ZnO was favored. The decisive role of the surface chemistry was confirmed by obtaining the selective formation of ZIF-8 films on substrates with ceramic surfaces under identical synthesis conditions. Furthermore, in water, the formation of the oxide film on copper surfaces was inhibited. However the growth kinetics of the ZIF-8 film was still low. In contrast, using a methanol-based mixture in the presence of acetate, the precursor-support interactions were favored leading to a selective growth of continuous, uniform and adherent ZIF-8 films on copper substrates. These films totally and uniformly covered the foils and exhibited partial crystallographic orientations on the {110} and {211} planes. Moreover, ZIF-8 films had good mechanical stability remaining firmly bonded to the substrate and also good thermal stability, preserving their physicochemical characteristics up to about 350 °C. The information obtained has implications in the development of new structured catalysts based on films of this MOF.

Acknowledgments

The authors wish to acknowledge the financial support received from Consejo Nacional de Investigaciones Científicas y Técnicas (CONICET), Agencia Nacional de Promoción Científica y Tecnológica (ANPCyT) and Universidad Nacional del Litoral (UNL). Thanks are also given to ANPCyT for the purchase of the multitechnique instrument SPECS (PME8-2003), to JICA for the XRD equipment, to Lic. Fernanda Mori for the collaboration in XPS and to Prof. Elsa Grimaldi for the English language editing.

Appendix A. Supplementary data

Supplementary data related to this article can be found at http://dx.doi.org/10.1016/j.micromeso.2015.02.049.

References

[1] J. Rowsell, O. Yagui, Microporous Mesoporous Mater. 73 (1–2) (2004) 3–14.
[2] G. Férey, Chem. Soc. Rev. 37 (1) (2008) 191–214.
[3] S. Meek, J. Greathouse, M. Allendorf, Adv. Mater. 23 (2) (2011) 249–267.
[4] Y. Li, F. Liang, H. Bux, A. Feldhoff, W. Yang, J. Caro, Angew. Chem. Int. Ed. 49 (2010) 548–551.
[5] B. Seoane, J. Zamaro, C. Tellez, J. Coronas, RSC Adv. 1 (2011) 917–922.
[6] P. Horcajada, R. Gref, T. Baati, P. Allan, G. Maurin, P. Couvreur, G. Férey, R. Morris, C. Serre, Chem. Rev. 112 (2) (2012) 1232–1268.
[7] L. Kreno, K. Leong, O. Farha, M. Allendorf, R. Van Duyne, J. Hupp, Chem. Rev. 112 (2) (2012) 1105–1125.
[8] A. Corma, H. García, F. Llabrés i Xamena, Chem. Rev. 110 (2010) 4606–4655.
[9] D. Farrusseng, S. Aguado, C. Pinel, Angew. Chem. Int. Ed. 48 (2009) 2–14.
[10] A. Phan, C. Doonan, F. Uribe-Romo, C. Knobler, M. O'Keeffe, O. Yaghi, Acc. Chem. Res. 43 (2010) 58–67.
[11] K. Park, Z. Ni, A. Coté, J. Choi, R. Huang, F. Uribe-Romo, H. Chae, M. ÓKeeffe, O. Yagui, PNAS 103 (2006) 10186–10191.
[12] D. Fairen-Jimenez, S. Moggach, M. Wharmby, P. Wright, S. Parsons, T. Düren, J. Am. Chem. Soc. 133 (2011) 8900–8902.
[13] A. Bétard, R. Fischer, Chem. Rev. 112 (2012) 1055–1083.
[14] M. Shah, M. McCarthy, S. Sachdeva, A. Lee, H. Jeong, Ind. Eng. Chem. Res. 51 (2012) 2179–2199.
[15] M. McCarthy, V. Varela-Guerrero, G. Barnett, H. Jeong, Langmuir 26 (18) (2010) 14636–14641.
[16] M. Shah, H. Kwon, V. Tran, S. Sachdeva, H. Jeong, Microporous Mesoporous Mater. 165 (2013) 63–69.
[17] K. Tao, C. Kong, L. Chen, Chem. Eng. J. 220 (2013) 1–5.
[18] H. Kwon, H. Jeong, J. Am. Chem. Soc. 135 (2013) 10763–10768.
[19] J. Yao, L. Li, W. Wong, C. Tan, D. Dong, H. Wang, Mater. Chem. Phys. 139 (2013) 1003–1008.
[20] H. Bux, F. Liang, Y. Li, J. Cravillon, M. Wiebcke, J. Caro, J. Am. Chem. Soc. 131 (2009) 16000–16001.
[21] L. Diestel, H. Bux, D. Wachsmuth, J. Caro, Microporous Mesoporous Mater. 164 (2012) 288–293.
[22] Y. Pan, B. Wang, Z. Lai, J. Membr. Sci. 421–422 (2012) 292–298.
[23] L. Li, J. Yao, R. Chen, L. He, K. Wang, H. Wang, Microporous Mesoporous Mater. 168 (2013) 15–18.
[24] S. Venna, M. Carreon, J. Am. Chem. Soc. 132 (2010) 76–78.
[25] H. Bux, C. Chmelik, R. Krishna, J. Caro, J. Membr. Sci. 369 (2011) 284–289.
[26] H. Bux, A. Feldhoff, J. Cravillon, M. Wiebcke, Y. Li, J. Caro, Chem. Mater. 23 (2011) 2262–2269.
[27] G. Xu, J. Yao, K. Wang, L. He, P. Webley, C. Chen, H. Wang, J. Membr. Sci. 385–386 (2011) 187–193.
[28] Y. Pan, T. Li, G. Lestari, Z. Lai, J. Membr. Sci. 390–391 (2012) 93–98.
[29] L. Fan, M. Xue, Z. Kang, H. Li, S. Qiu, J. Mater. Chem. 22 (2012) 25272–25276.
[30] K. Kida, K. Fujita, T. Shimada, S. Tanaka, Y. Miyake, Dalton Trans. 42 (31) (2013) 11128–11135.
[31] D. Nagaraju, D. Bhagat, R. Banerjee, U. Kharul, J. Mater. Chem. A 1 (31) (2013) 8828–8835.
[32] L. Dumée, L. He, M. Hill, B. Zhu, M. Duke, J. Schütz, F. She, H. Wang, S. Gray, P. Hodgson, L. Kong, J. Mater. Chem. A 1 (2013) 9208–9214.
[33] M. He, J. Yao, L. Li, Z. Zhong, F. Chen, H. Wang, Microporous Mesoporous Mater. 179 (2013) 10–16.
[34] G. Lu, J. Hupp, J. Am. Chem. Soc. 132 (2010) 7832–7833.
[35] R. Jin, Z. Bian, J. Li, M. Ding, L. Gao, Dalton Trans. 42 (2013) 3936–3940.
[36] G. Groppi, G. Airoldi, C. Cristiani, E. Tronconi, Catal. Today 60 (2000) 57–62.

[37] J. Zamaro, E. Miró, in: M. Naboka, J. Giordano (Eds.), Copper Alloys: Preparation, Properties and Applications, Nova Science Publishers Inc., New York, 2011, pp. 127–139.
[38] N. Pérez, E. Miró, J. Zamaro, Appl. Catal. B 129 (2013) 416–425.
[39] J. Camra, E. Bielanska, A. Bernasik, K. Kowalski, M. Zimowska, A. Białas, M. Najbar, Catal. Today 105 (3–4) (2006) 629–633.
[40] Y. Pan, D. Heryadi, F. Zhou, L. Zhao, G. Lestari, H. Su, Z. Lai, Cryst. Eng. Comm. 13 (2011) 6937–6940.
[41] E. Bustamante, J. Fernández, J. Zamaro, J. Colloid Interface Sci. 424 (2014) 37–43.
[42] J. Cravillon, S. Münzer, S. Lohmeier, A. Feldhoff, K. Huber, M. Wiebcke, Chem. Mater. 21 (2009) 1410–1412.
[43] J. Zamaro, M. Ulla, E. Miro, Appl. Catal. A 308 (2006) 161–171.
[44] J. Verduijn, A. Bons, M. Anthonis, L. Czarnetzki, Int. Pat. Appl. PCT WO 96/01683.
[45] J. Caro, M. Noack, P. Kolsch, R. Schafer, Microporous Mesoporous Mater. 38 (2000) 3–24.
[46] T. Muster, I. Cole, Corros. Sci. 46 (2004) 2319–2335.
[47] S. Mei, J. Yang, J. Ferreira, J. Colloid Interface Sci. 241 (2001) 417–421.
[48] Y. Zhao, W. Xing, N. Xub, F. Wong, Sep. Purif. Technol. 42 (2005) 117–121.
[49] Health and Safety Guide N° 43 in Environmental Health Criteria 114: Dymethylformamide (DMF), World Health Organization, 1990.
[50] T. Soejima, H. Yagyu, N. Kimizuka, S. Ito, RCS Adv. 1 (2011) 187–190.
[51] J. Leahy, C. Macken, M. Ryan, J. Colloid Interface Sci. 225 (2000) 209–213.
[52] H. Chen, L. Wang, J. Yang, R. Yang, J. Phys. Chem. C 117 (2013) 7565–7576.
[53] NIST X-ray Photoelectron Spectroscopy Database, http://srdata.nist.gov/xps.
[54] F. Tian, A. Cerro, A. Mosier, H. Wayment-Steele, R. Shine, A. Park, E. Webster, L. Johnson, M. Johal, L. Benz, J. Phys. Chem. C 118 (2014) 14449–14456.
[55] M. Biesinger, L. Lau, A. Gerson, R. Smart, Appl. Surf. Sci. 257 (2010) 887–898.